# Electronic Supplementary Information for:

## Long-lived charge separation state in spiro-compact rhodamine–naphthalenediimide D–A–D systems: synthesis and time-resolved optical and electron paramagnetic resonance spectroscopic studies

Balamurugan Tharmalingam,‡[a] Andrey A. Sukhanov,‡[b] Yuying Pei,[a] Greta Sambucari,[cd] Talita Ramos,[cd] Jianzhang Zhao,*[a] Violeta K. Voronkova,*[b] and Mariangela Di Donato *[ce]

[a] State Key Laboratory of Fine Chemicals, Frontier Science Center for Smart Materials, School of Chemical Engineering, Dalian University of Technology, Dalian 116024 (P. R. China). *E-mail: zhaojzh@dlut.edu.cn

[b]Zavoisky Physical-Technical Institute, FRC Kazan Scientific Center of Russian Academy of Sciences, Kazan 420029, Russia. *E-mail: vor18@yandex.ru (V.K.V)

[c]LENS (European Laboratory for Non-Linear Spectroscopy) via N. Carrara 1, 50019 Sesto Fiorentino (FI) Firenze, Italy. *E-mail : didonato@lens.unifi.it (M.D.D)

[d]INO-CNR, via N.Carrara 1, 50019 Sesto Fiorentino (FI) Firenze, Italy

[e]ICCOM-CNR, via Madonna del Piano 10, 50019, Sesto Fiorentino (FI), Italy

**Contents**

## 1. Experimental Section

**1.1. Materials and Methods.** All materials used for synthesis are of analytical purity. The synthesis of starting compounds is based on the previous literature methods for preparation of Rhodamine B hydrazide (**RB-1**), Rhodamine B ethylenediamine (**RB-2**)[1] and *N*-(2-ethylhexyl)naphthalene-1,4,5,8-tetracarboxylic monoanhydride monoimide (**NDI-1**).[2] For samples requiring a $N_2$ atmosphere during measurement, the solution was purged with $N_2$ for 15 minutes before the measurement. $^1$H NMR spectra were recorded on Bruker Avance 400 MHz. UV–vis absorption spectra were obtained using a UV–2550 spectrophotometer (Shimadzu Ltd, Japan). Fluorescence emission spectra were recorded using an FS5 spectrofluorometer (Edinburgh Instruments, U.K.).

**1.2. Synthesis of Rho-NDI-Rho.** Under a $N_2$ atmosphere, rhodamine B hydrazide (170 mg, 0.37 mmol) and 1,4,5,8-naphthalenetetracarboxylic acid anhydride (50 mg, 0.18 mmol) were dissolved in acetic acid (5 mL). The reaction mixture was refluxed and stirred for 24 hours. The progress of the reaction was monitored by TLC (thin-layer chromatography as eluent dichloromethane (DCM)/methanol (MeOH) = 30:1, v/v). After completion of the reaction, the mixture was cooled to room temperature. The reaction mixture was then poured into ice-water mixture. The pH of the resulting solution was adjusted to 8−9 by adding 1M NaOH aqueous solution. A purple solid precipitate formed, which was filtered and washed with cold water several times. The resulting solid was dried under vacuum. The crude compound was further purified by column chromatography (silica gel, DCM/MeOH = 30:1, v/v) to give **Rho-NDI-Rho** as purple color solid (84 mg, yield: 27%). M.p.: 232.5−233.2 °C. $^1$H NMR (400 MHz, $CDCl_3$) δ: 8.31 (s, 4H), 8.08 (d, *J* = 4 Hz, 2H), 7.70−7.64 (m, 4H), 7.40 (d, *J* = 8 Hz, 2H), 6.76−6.68 (m, 4H), 6.68−6.38 (m, 4H), 6.14 (d, 4H), 3.29−3.22 (m, 16H), 1.31−1.19 (m, 24H). $^{13}$C NMR (125 MHz, $CDCl_3$): δ164.41, 160.09, 154.72, 149.11, 131.18, 130.73, 130.59, 128.89, 127.06, 124.90, 123.97, 108.09, 108, 105.52, 105.46, 97.55, 97.44, 67.99, 44.65, 38.31, 32.03, 22.79, 14.43, 12.12. TOF-MALDI-HRMS: calculated for ($[C_{70}H_{64}N_8O_8 + H]^+$), *m/z* = 1145.4919; found: 1145.4888.

**1.3. Synthesis of Rho-CH-NDI. Rho-CH-NDI** was prepared with a method similar to that used for **Rho-NDI-Rho.** Where **RB-2** (50 mg, 0.20 mmol) and **NDI-1** (50 mg, 0.20 mmol) were dissolved in acetic acid (5 mL). **Rho-CH-NDI** was obtained as a red solid (13 mg, yield 10%). M.p.: 222.3−

224.5 °C. $^{1}$H NMR (400 MHz, $CDCl_3$) δ: 8.76−8.63 (m, 4H), 7.88 (s, 1H), 7.42 (s, 2H), 7.0 (s, 1H), 6.40−6.33 (dd, 3H), 5.91 (s, 2H), 4.15−4.13 (dd, 4H), 3.60−3.53 (m, 2H), 3.11 (s, 8H), 2.38−2.34 (m, 1H), 1.38−1.25 (m, 8H), 1.17−1.07 (m, 12H), 0.94−0.88 (m, 7H). $^{13}$C NMR (125 MHz, $CDCl_3$): δ 163.25, 162.78, 131.45, 130.98, 130.84, 130.63, 129.70, 128.45, 126.74, 123.73, 44.49, 44.29, 37.99, 30.66, 29.63, 28.57, 23.97, 23.01, 22.63, 14.06, 14.03, 10.55. TOF-MALDI-HRMS calculated for ($[C_{52}H_{55}N_5O_6 + H]^+$), *m/z* = 845.4152; found: 845.4187.

**1.4. Synthesis of Rho-CH-NDI-CH-Rho. Rho-CH-NDI-CH-Rho** was prepared with a similar method to that used for **Rho-NDI-Rho.** Here **RB-2** (180 mg, 0.37 mmol) and 1,4,5,8-naphthalenetetracarboxylic acid anhydride (50 mg, 0.18 mmol) were dissolved in acetic acid (5 mL). **Rho-CH-NDI-CH-Rho** was obtained as a red solid (Yield of 80 mg, 30%). M.p.: 207.1−208.3 °C. $^{1}$H NMR (400 MHz, $CDCl_3$) δ: 8.56 (s, 4H), 7.89−7.87 (m, 2H), 7.41−7.39 (m, 3H), 7.0 (s, 2H), 6.40−6.38 (m, 4H), 6.27 (s, 4H), 5.92 (s, 4H), 4.27 (s, 4H), 3.51−3.49 (m, 4H), 3.11 (s, 16H), 1.11−1.05 (m, 24H). $^{13}$C NMR (125 MHz, $CDCl_3$): δ 169.08, 162.97, 153.62, 148.55, 132.50, 131.49, 130.50, 129.05, 128.16, 126.79, 126.68, 124.03, 123.05, 108.10, 105.80, 97.94, 65.49, 44.32, 39.72, 39.33, 32.06, 25.14, 24.92, 22.83, 14.26, 12.10. TOF-MALDI-HRMS calculated for ($[C_{74}H_{72}N_8O_8 + H]^+$), *m/z* = 1201.5556; found: 1201.5572.

**1.5. Single Crystal X-ray Diffraction.** The triads were characterized through single-crystal X-ray diffraction, using crystals obtained via the slow diffusion of DMF into an ACN solution. X-ray diffraction data for these crystals were collected at 298 K using a Bruker D8 Venture CMOS-based diffractometer with graphite monochromatized Kα radiation (λ = 0.71073 Å). The SMART and SAINT programs were used for data collection, and the SheIXT structure solution was applied through intrinsic phasing. The data were refined using the SheIXL refinement package with least squares minimization in Olex2.[3] CCDC 2370986 (**Rho-NDI-Rho**) and 2370987 (**Rho-CH-NDI-CH-Rho)** contain the supplementary crystallographic data for this paper, and the data can be obtained freely from the Cambridge Crystallographic Data Centre via https://www.ccdc.cam.ac.uk/.

**1.6. Nanosecond Transient Absorption Spectroscopy.** The nanosecond transient absorption (ns-TA) spectra were obtained using the LP980 laser flash photolysis spectrometer from Edinburgh Instruments, U.K. Before measurements, all sample solutions were purged with $N_2$ for approximately 20 minutes. Excitation was provided by a nanosecond pulsed laser, and the signals were digitized with a Tektronix TDS 3012B oscilloscope. The sample was excited by 355 nm

nanosecond pulsed laser. The nanosecond pulsed laser used for excitation was the surelite I-10, USA, the wavelength is tunable in the range of 210-2400 nm. The typical laser pulse energy was 10 mJ per pulse. Data analysis was conducted using L900 software.

**1.7. Density Functional Theory (DFT) Calculations.** The geometries of the dyads were optimized using Density Functional Theory (DFT) with the B3LYP functional and the 6-31G(d) basis set. The excited triplet state energy was calculated using Time-Dependent Density Functional Theory (TDDFT) with the same functional and basis set, based on the optimized ground-state geometry. All calculations were performed using Gaussian 16 software.[4]

**1.8. Femtosecond Transient Absorption Spectroscopy.** The femtosecond transient absorption spectra were recorded on a system based on Ti laser amplifier optical parametric amplifier system (Coherent Legend Elite) with a 40-fs pulse duration and 1 kHz repetition rate. The pump beam at 350 nm was selected based on the steady-state absorption spectra of the studied compounds and was produced as the third harmonic generation of the signal output of a commercial optical parametric amplifier (TOPAS, Light Conversion) pumped by the fundamental laser radiation. The probe beam was generated by focusing a small portion of the fundamental laser radiation on a 3 mm thick $CaF_2$ crystal. The data were analyzed with a global analysis procedure using the software Glotaran-1.5.1.[5]

**1.9. Time-Resolved Electron Paramagnetic Resonance (TREPR) Spectra.** Steady-state electron paramagnetic resonance (EPR) spectroscopy measurements were conducted at 300 K using an X-band (9.4 GHz) EPR ELEXSYS E500 spectrometer (Bruker, Germany). The radical anion of the dyad/triads was produced by adding a reductant of tetrabutylammonium fluoride (TABF) into deoxygenated *N,N*-dimethylformamide (DMF), after which the EPR quartz tube was sealed with an $H_2/O_2$ torch under a $N_2$ atmosphere. Time-resolved TREPR measurements were conducted at 80 K and 298 K using an X-band EPR spectrometer based on a Bruker EMX (Germany). Samples were dissolved in a 3:1 (v/v) mixture of TOL and 2-MeTHF, with oxygen removed through five freeze-pump-thaw cycles. The spectra were simulated using the EasySpin package based on Matlab.[6]

## 2. NMR and HRMS Spectra data.

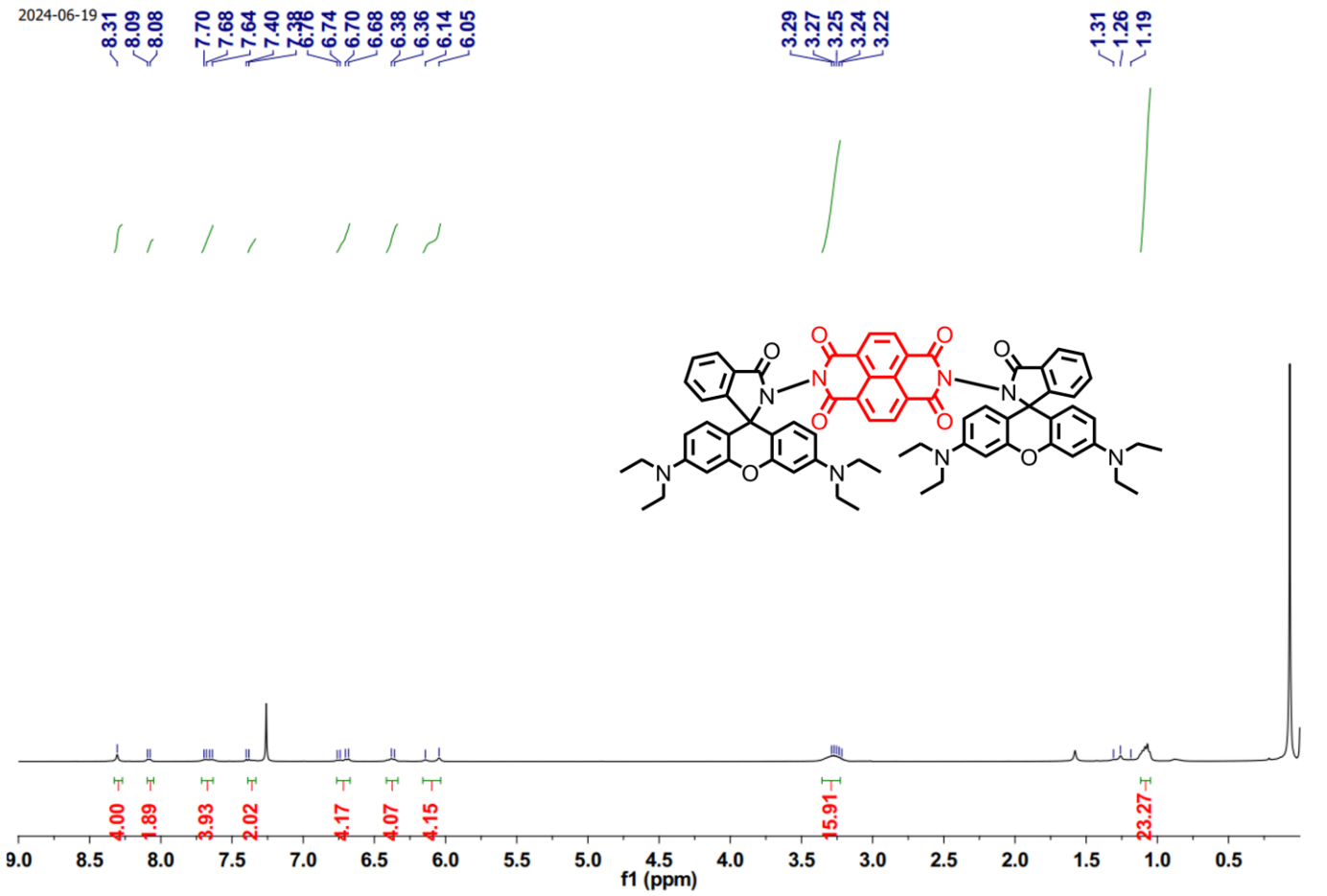


**Figure S1.** $^{1}$H NMR spectrum of **Rho-NDI- Rho** ($CDCl_3$, 400 MHz).

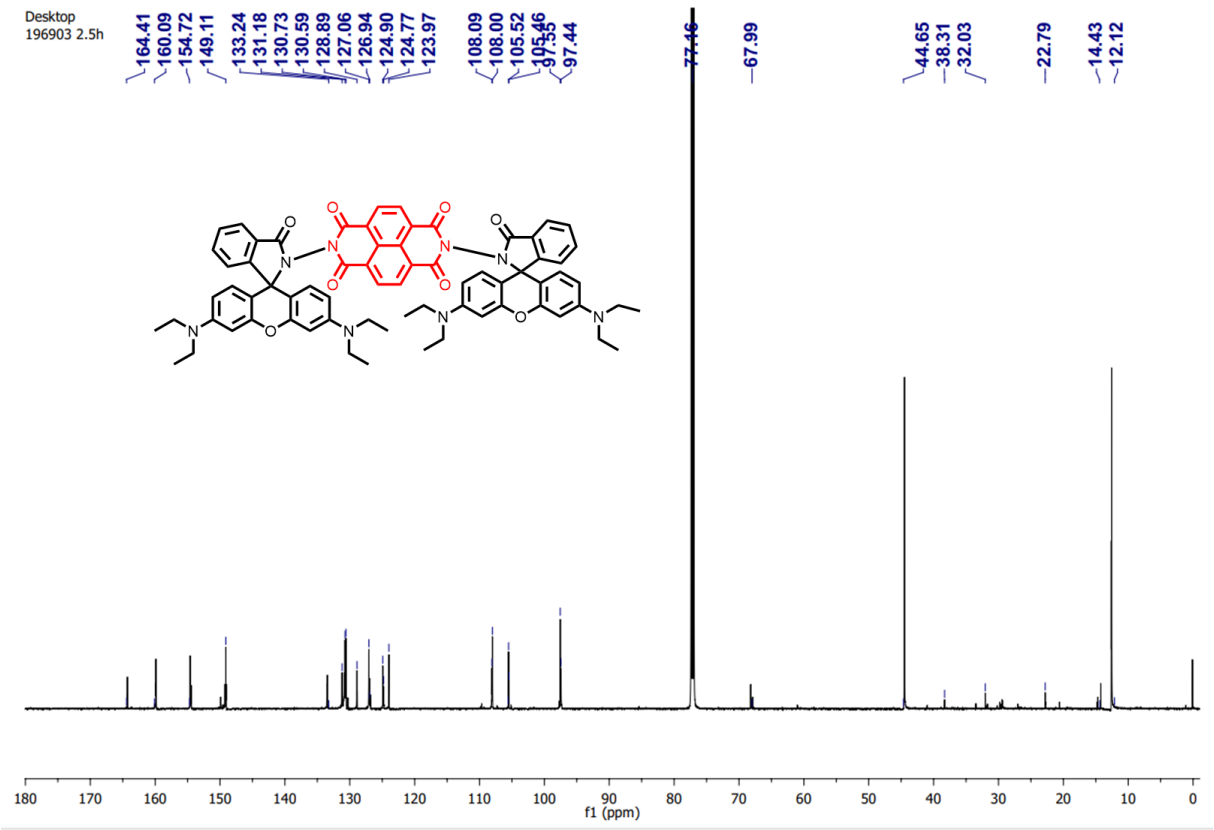


**Figure S2**. $^{13}C$ NMR spectrum of **Rho-NDI-Rho** ($CDCl_3$, 125 MHz).

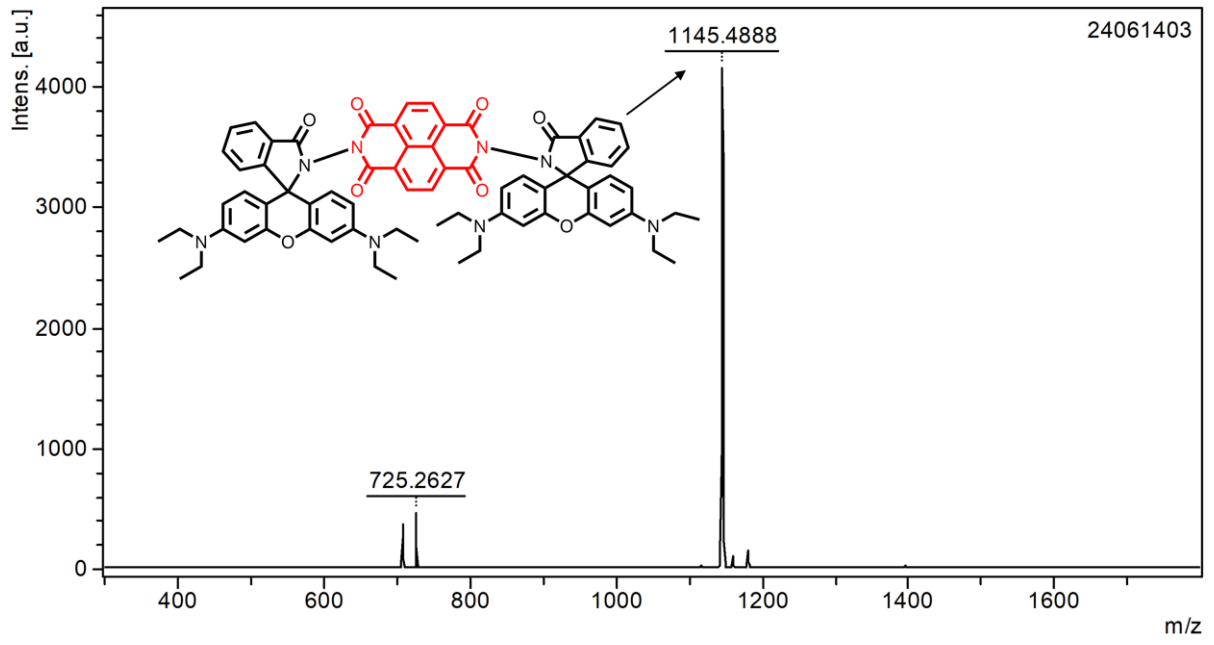


**Figure S3.** MALDI-TOF-HRMS high resolution mass spectrum of **Rho-NDI-Rh0**.

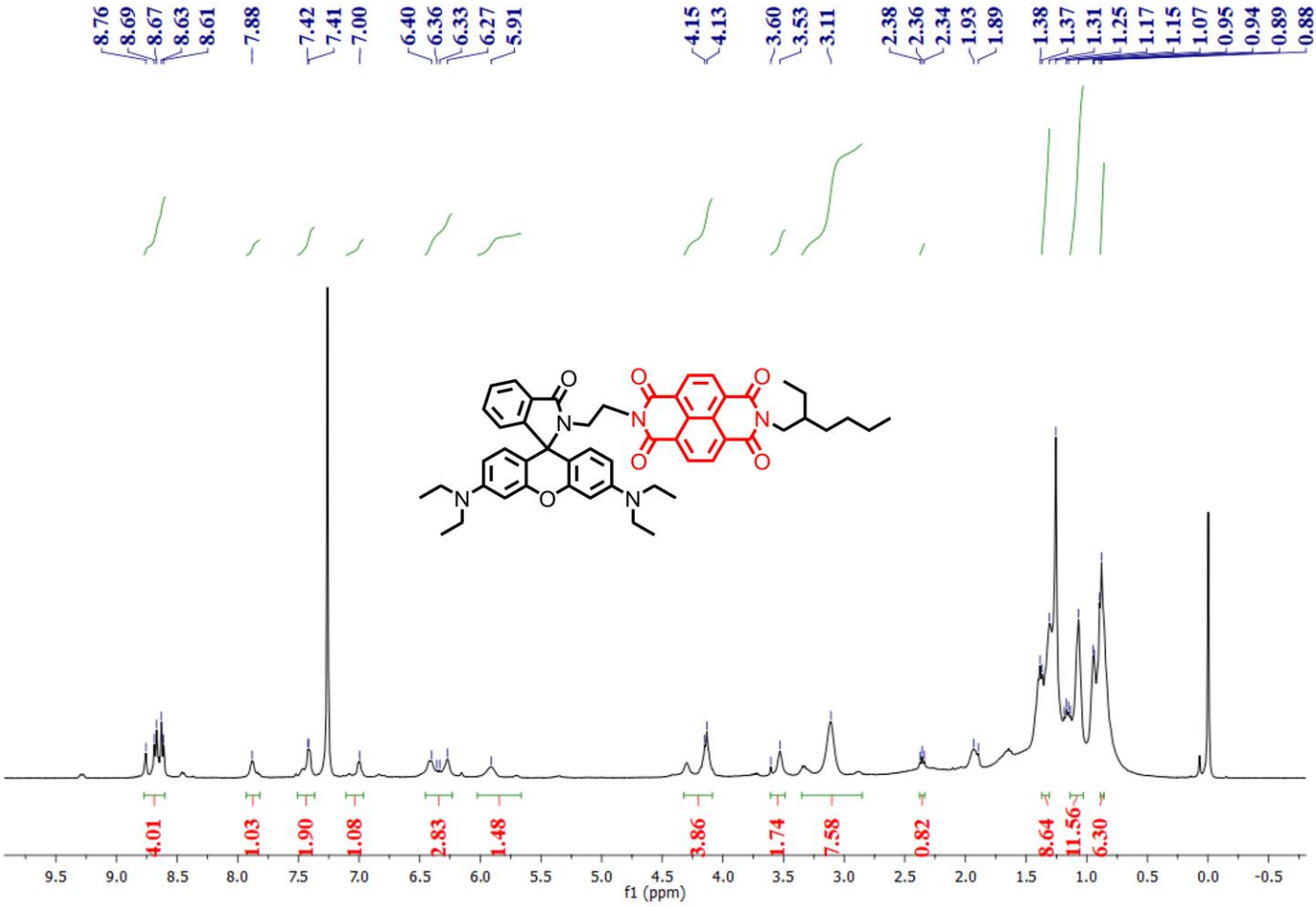


**Figure S4.** $^{1}$H NMR spectrum of **Rho- CH-NDI** ($CDCl_3$, 125 MHz).

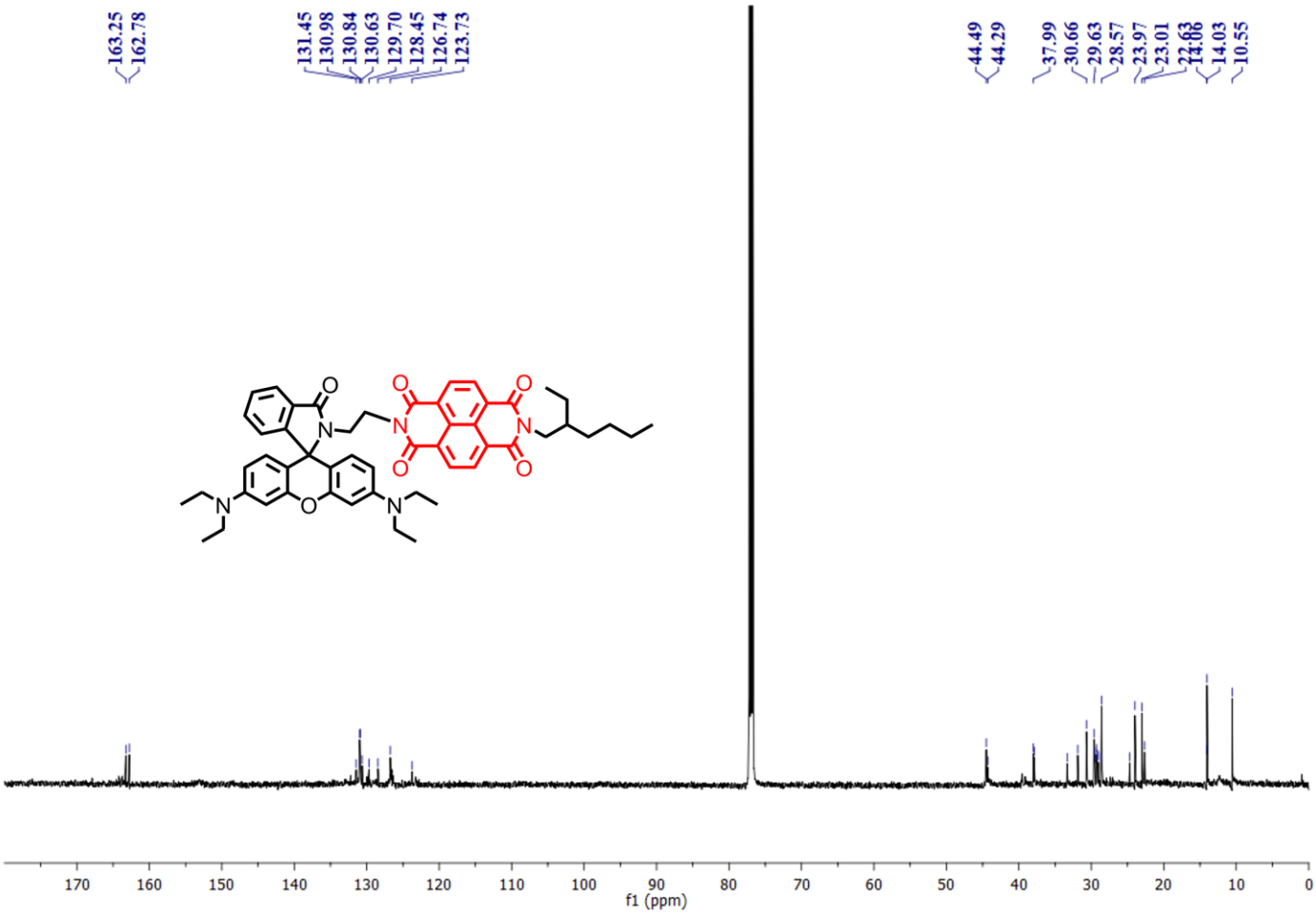


**Figure S5**. $^{13}C$ NMR spectrum of **Rho-CH-NDI** (400 MHz, $CDCl_3$).

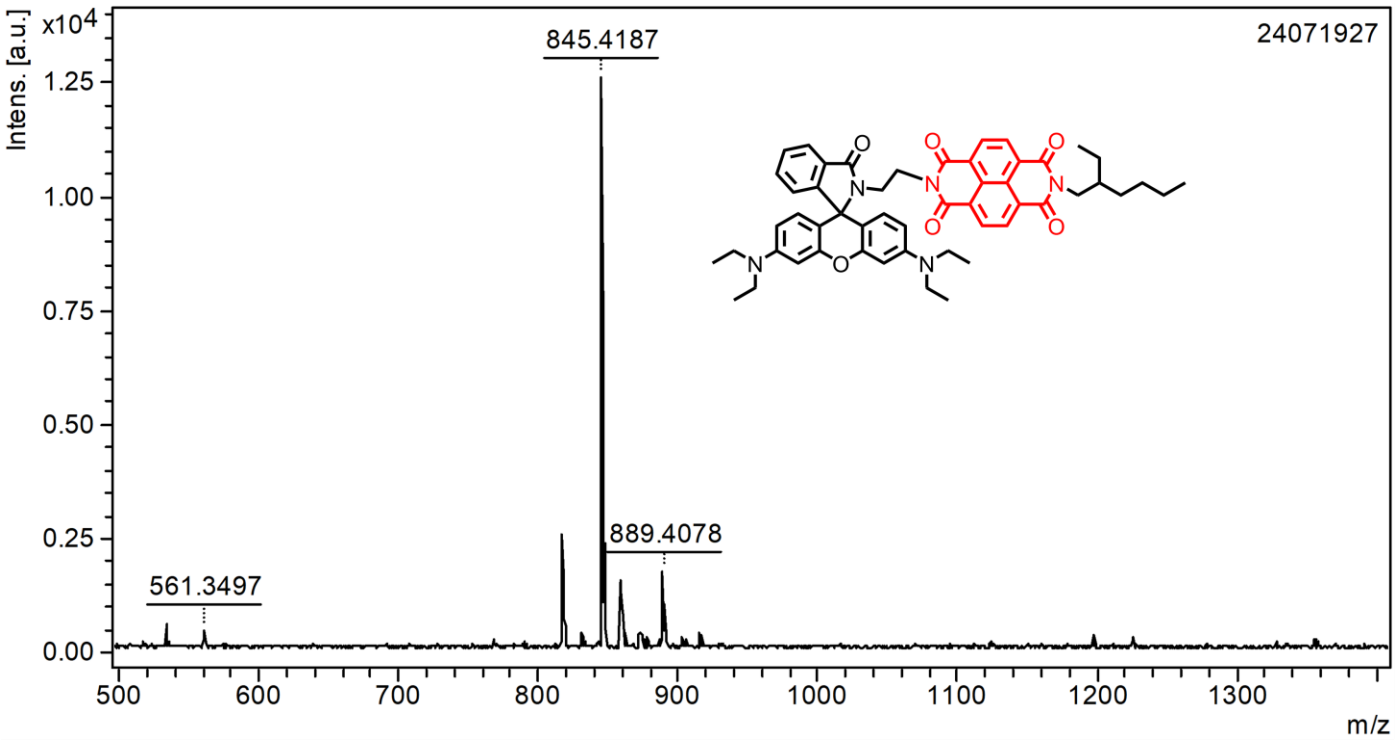


**Figure S6**. MALDI-TOF-HRMS high resolution mass spectrum of **Rho-CH-NDI**.

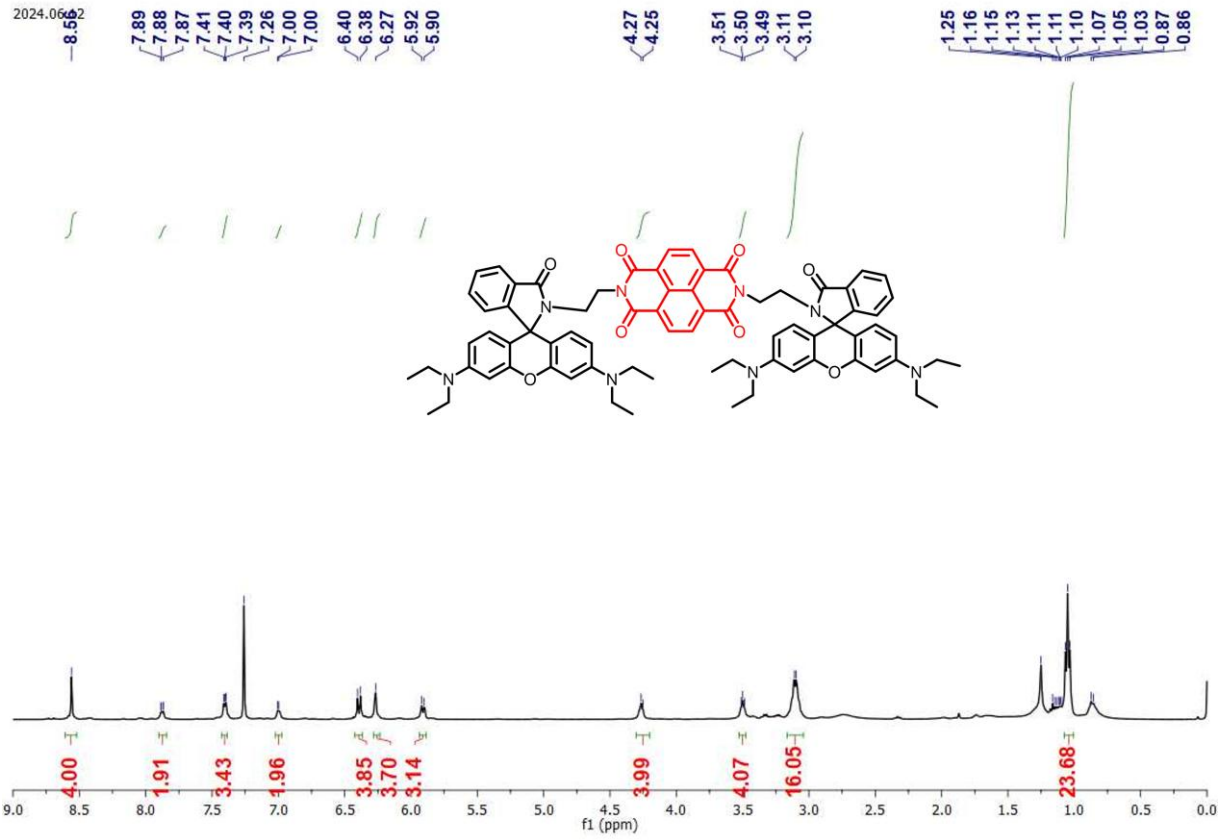


**Figure S7.** $^{1}$H NMR spectrum of **Rho-CH-NDI-CH-Rho** ($CDCl_3$, 400 MHz).

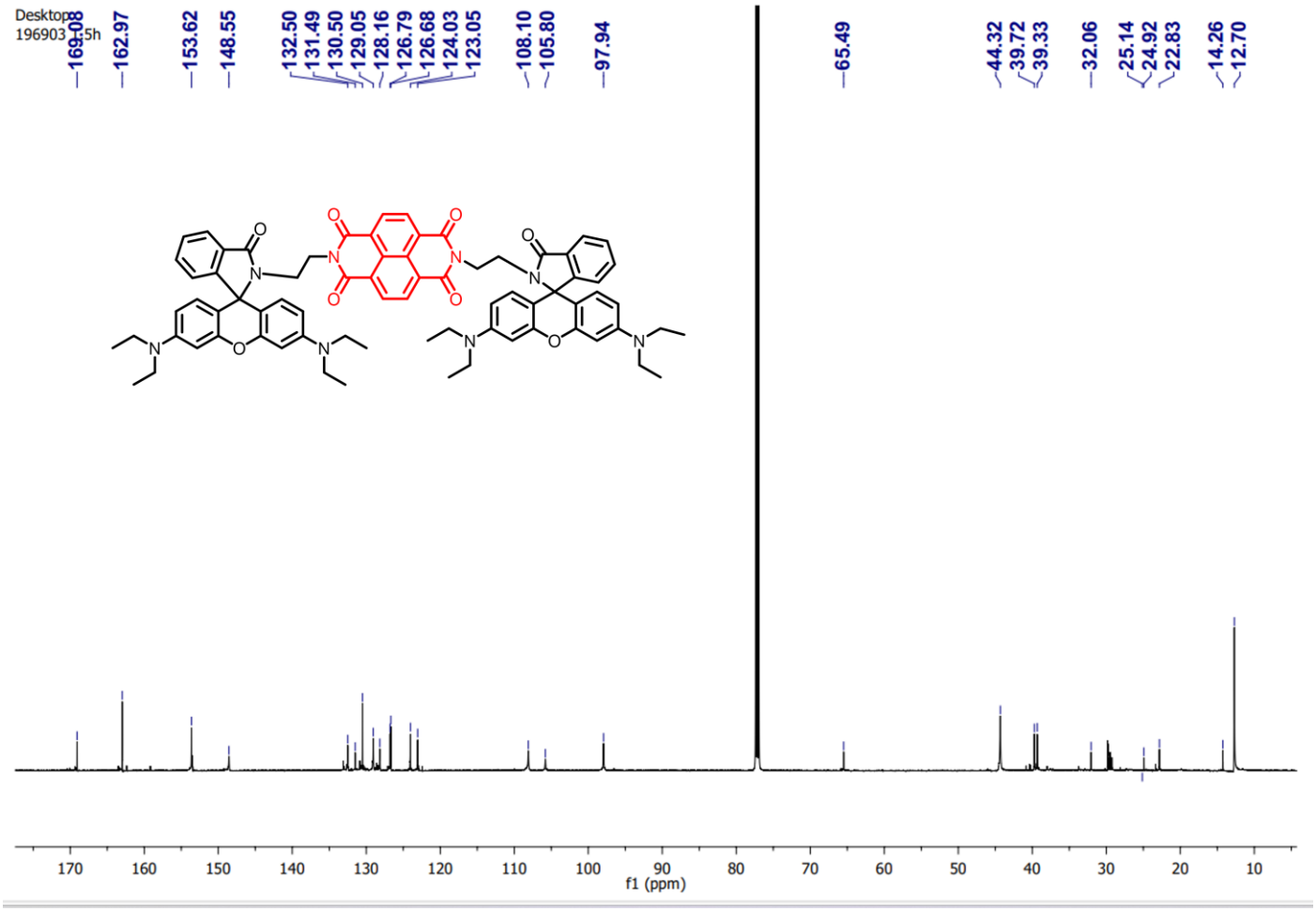


**Figure S8.** $^{13}C$ NMR spectrum of **Rho-$CH_2$-NDI- $CH_2$-Rho** ($CDCl_3$, 125 MHz).

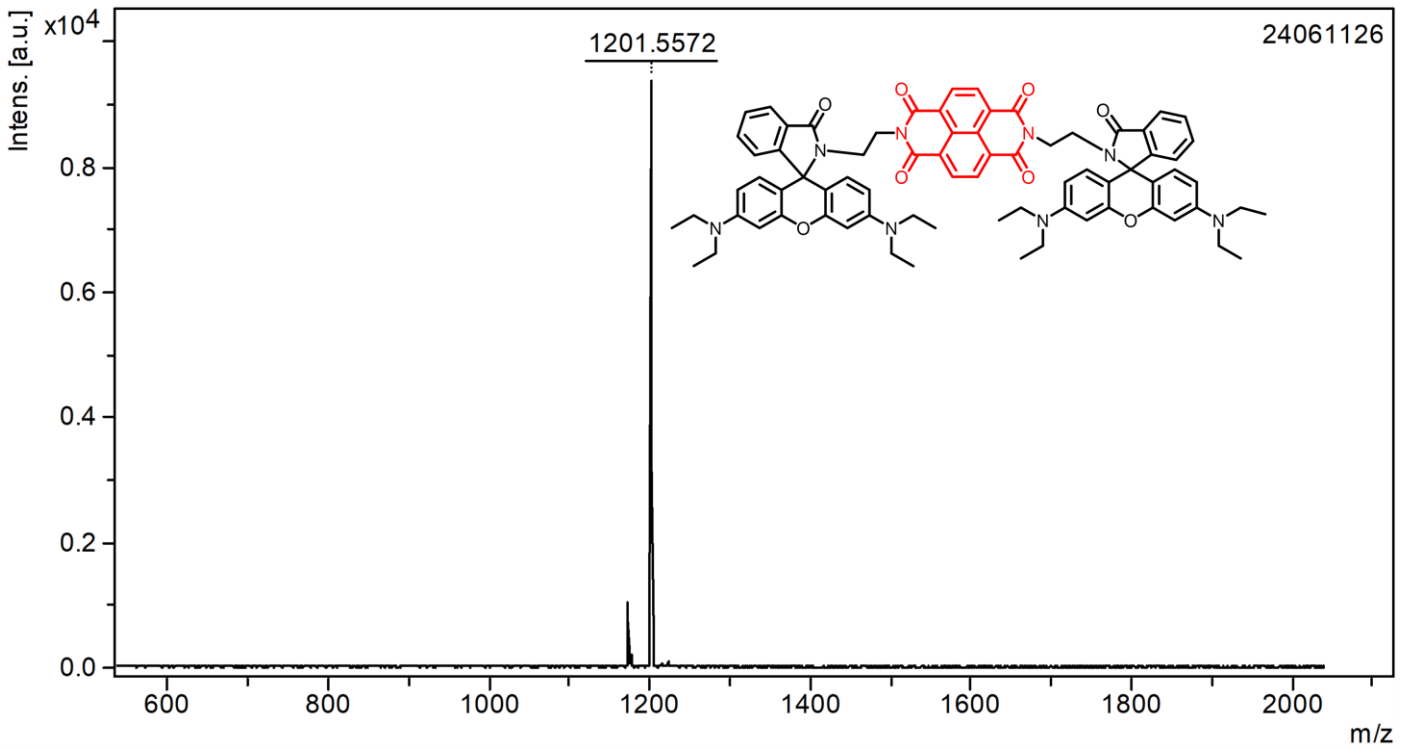


**Figure S9.** MALDI-TOF-HRMS high resolution mass spectrum of **Rho-CH-NDI- CH-Rho**.

## 3. Crystallographic Data

**Table S1. Crystallographic Data of Rho-NDI-Rho and Rho-CH-NDI-CH-Rho**

| Compound | **Rho-NDI-Rho** | **Rho-CH-NDI-CH-Rho** |
|---|---|---|
| Empirical formula | $C_{70}$ $H_{64}N_8O_8$ | $C_{74}H_{72}N_8O_8$,2($C_2H_3N$), |
| Formula weight | 1145.29 | 1283.50 |
| Temperature | 126 K | 150 K |
| Wavelength | 0.71073 Å | 0.71073 Å |
| Crystal system | Monoclinic | Triclinic |
| Space group | P-21/n | P-1 |
| Unit cell dimensions | a = 15.695(2) Å<br>b = 11.561(18) Å<br>c = 18.283(3) Å<br>α = 90°<br>β = 106.336(18)°<br>γ = 90° | a= 12.294(2) Å<br>b = 13.387(2) Å<br>c = 20.532(3) Å<br>α = 86.872(6)°<br>β = 87.845(5)°<br>γ = 83.021 (6)° |
| Volume | 3183.8(8) $Å^3$ | 3347.7(9) $Å^3$ |
| Z | 2 | 2 |
| Density (calculated) | 1.195 $Mg/m^3$ | 1.273 $Mg/m^3$ |
| Absorption coefficient | 0.079 $mm^{-1}$ | 0.084 $mm^{-1}$ |
| F(000) | 1208 | 1360 |
| Data completeness | 0.99 | 0.97 |
| Absorption correction | None | None |
| Goodness-of-fit on F2 | 1.031 | 1.016 |
| R [a] | 0.0659 | 0.0635 |
| $\omega R^2$ [a] | 0.1539 | 0.1883 |

[a] $R = \sum ||F_o| - |F_c|| / \sum |F_o|, \omega R_2 = [\sum_W (F_o^2 - F_c^2)^2 / \sum_W (F_o^2)^2]^{\frac{1}{2}}; |F_o| > 4\sigma(|F_o|)$.

## 4. UV-vis absorption Spectra

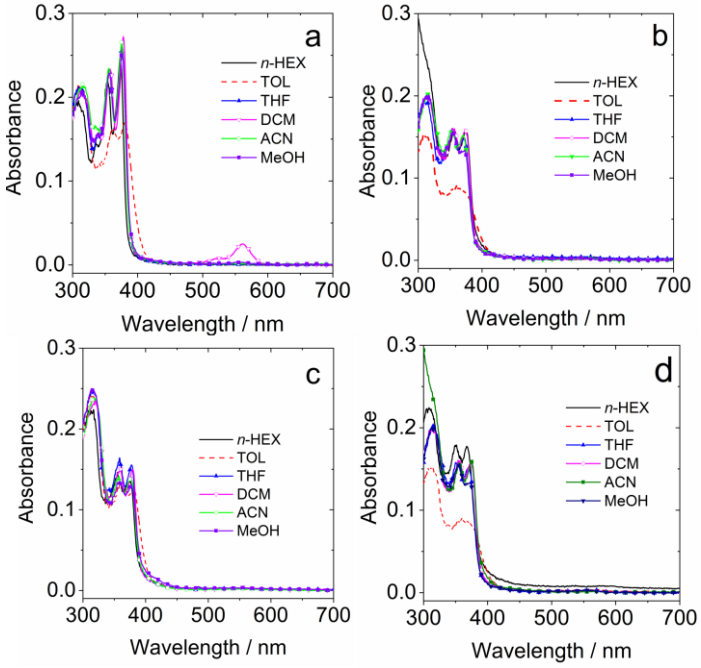


**Figure S10.** UV–vis absorption spectra of (a) **Rho-NDI** (b) **Rho-NDI-Rho** (c) **Rho-CH-NDI** (d) **Rho-CH-NDI-CH-Rho** in $c = 1.0 \times 10^{-5}$ M, 25 °C.

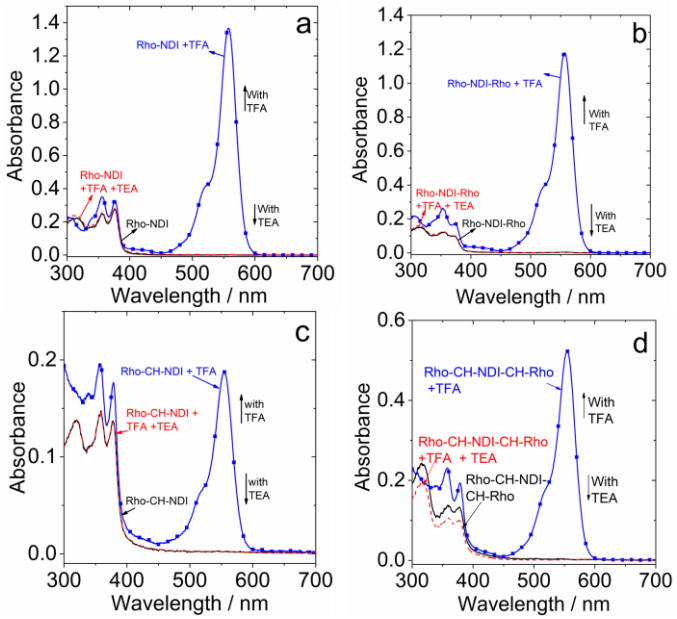


**Figure S11.** UV–vis absorption spectra of (a) **Rho-NDI** (b) **Rho-NDI-Rho** (c) **Rho-CH-NDI** (d) **Rho-CH-NDI-CH-Rho** with addition of TFA and TEA in MeOH $c = 1.0 \times 10^{-5}$ M, 25 °C.

## 5. Fluorescence Spectra

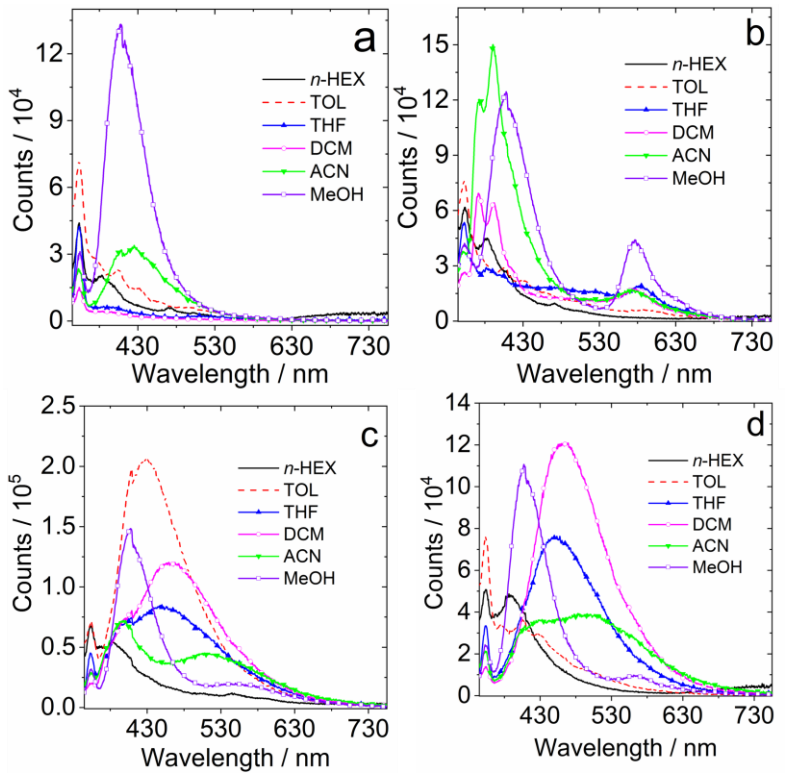


**Figure S12.** Fluorescence emission spectra of (a) **Rho-NDI** (b) **Rho-NDI-Rho** (c) **Rho-CH-NDI** (d) **Rho-CH-NDI-CH-Rho.** Optical mated solution was used all the solution shows same absorption at excitation wavelength.

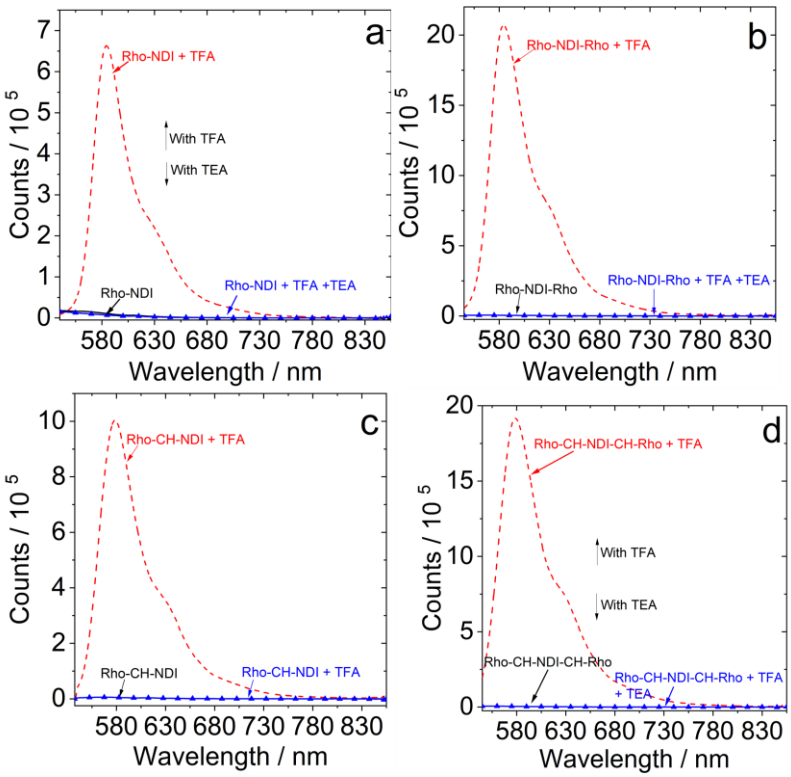


**Figure S13.** Fluorescence emission spectra of (a) **Rho-NDI** (b) **Rho-NDI-Rho** (c) **Rho-CH-NDI** (d) **Rho-CH-NDI-CH-Rho** with addition of TFA and TEA in MeOH $c = 1.0 \times 10^{-5}$ M, 25 °C.

**Table S2. Singlet Oxygen quantum yield of the Compounds in Different Solvents**[a]

| Compounds[a] | TOL | DCM | ACN | MeOH |
|---|---|---|---|---|
| **NDI** | 28.2 | 85.5 | 93.7 | 26.6 |
| **Rho-NDI** | 28.5 | 49.5 | 60.6 | 26.5 |
| **Rho-NDI-Rho** | *b* | *b* | *b* | *b* |
| **Rho-CH-NDI** | *b* | 46.1 | 25.3 | *b* |
| **Rho-CH-NDI-CH-Rho** | *b* | *b* | *b* | *b* |

[a] Singlet oxygen quantum yield ($^1O_2$) with $Ru(bpy)_3^{2+}$ as standard ($\Phi\Delta$ = 57% in DCM) in toluene. [b] Not observed.

**Table S3. Fluorescence Quantum Yields ($\Phi_F$ %) of the compounds in different solvents**

| Compounds | HEX | TOL | DCM | ACN |
|---|---|---|---|---|
| **NDI** | 0.4 | 0.5 | 0.3 | 0.3 |
| **Rho-Ph** | 1.2 | - | - | - |
| **Rho-NDI** | 0.2 | 0.3 | 0.1 | 0.1 |
| **Rho-NDI-Rho** | 0.1 | 0.1 | 0.1 | 0.1 |
| **Rho-CH-NDI** | 0.3 | 0.2 | 0.2 | 0.2 |
| **Rho-CH-NDI-CH-Rho** | 0.1 | 0.1 | 0.1 | 0.1 |

## 6. Electrochemical Studies

In Eqs. 2–5, ΔG represents the static Coulombic energy; $\Delta G^{\circ}_{CS}$ and $\Delta G^{\circ}_{CR}$ correspond to the Gibbs free energy changes associated with the charge separation and charge recombination processes, respectively. *E*css denotes the energy of the charge-separated state. Here, e is the electronic charge, $E_{OX}$ is the half-wave potential for one-electron oxidation of the donor unit, and $E_{RED}$ is the half-wave potential for one-electron reduction of the acceptor unit. $E_{00}$ refers to the singlet excited-state energy estimated from the UV–vis absorption maximum in hexane. The static dielectric constant of the solvent is expressed as $\varepsilon_s$, and $R_{CC}$ represents the donor–acceptor center-to-center distance, obtained from DFT-optimized geometries. The calculated $R_{CC}$ values are 6.3 Å for **Rho–NDI–Rho**, 6.8 Å for **Rho–CH–NDI**, and 6.8 Å for **Rho–CH–NDI–CH–Rho**. $R_D$ and $R_A$ denote the radius of the electron donor and acceptor, respectively, $\varepsilon_{REF}$ is the dielectric constant of the solvent used in electrochemical measurements, and ε0 is the permittivity of free space. The solvents employed in the free energy calculations were HEX ($\varepsilon_s$ = 1.88), TOL ($\varepsilon_s$ = 2.38), DCM ($\varepsilon_s$ = 8.93), and ACN, ($\varepsilon_s$ = 37.5).

## 7. Chemical Redox and Spectroelectrochemical Study

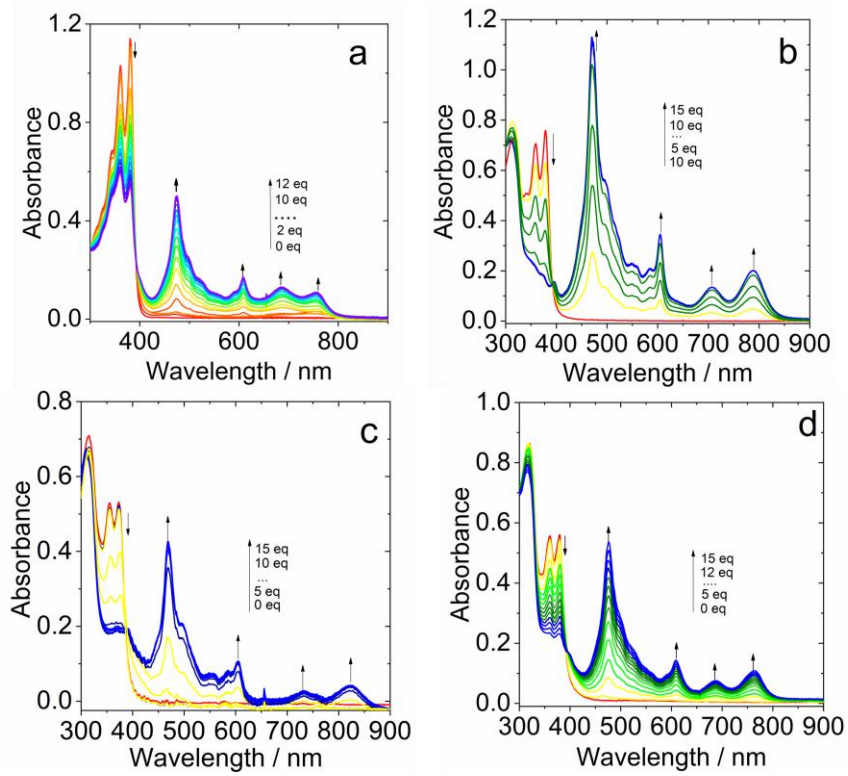


**Figure S14.** UV-vis absorption spectra of (a) **NDI**, (b) **Rho-NDI,** (c) **Rho-NDI-Rho** and (d) **Rho-CH-NDI-CH-Rho** chemically reduced with tetrabutylammonium fluoride (TABF) to generate $NDI^{-\bullet}$ in deaerated *N*,*N*-dimethylformamide. $c = 3.0 \times 10^{-5}$ M, 25 °C.

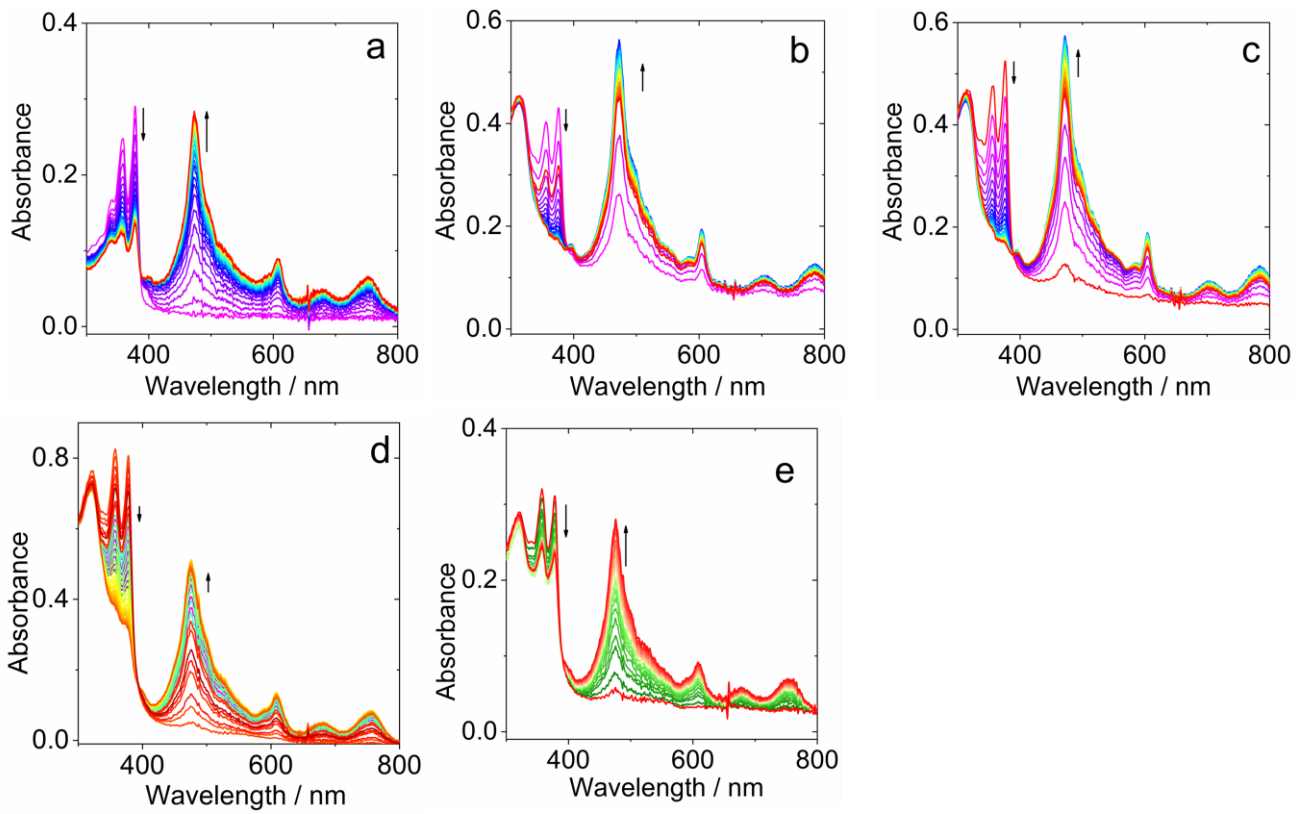


**Figure S15.** The spectroelectrochemistry study of (a) **NDI**, (b) **Rho-NDI**, (c) **Rho-NDI-Rho**, (d) **Rho-CH-NDI**, and (e) **Rho-CH-NDI-CH-Rho** by monitoring the evolution of UV-vis absorption upon a potential of -1.2 V (vs. $Ag/AgNO_3$) applied in deaerated ACN. The spectra were recorded in situ with a spectroelectrochemical cuvette (1 mm optical path). c = $3.0 \times 10^{-4}$ M, 25 °C.

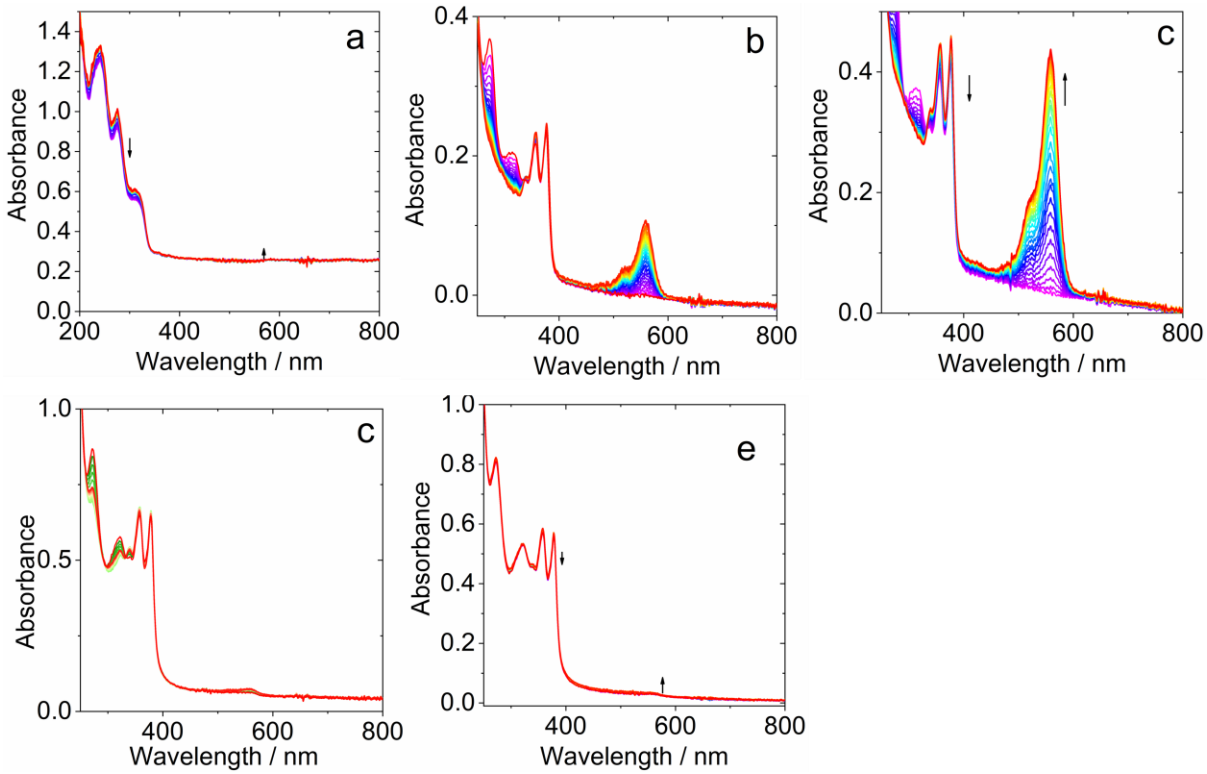


**Figure S16.** The spectroelectrochemistry study of (a) **Rho-Ph**, (b) **Rho-NDI**, (c) **Rho-NDI-Rho**, (d) **Rho-CH-NDI**, and (e) **Rho-CH-NDI-CH-Rho** by monitoring the evolution of UV-vis absorption upon a potential of 0.63 V (*vs.* $Ag/AgNO_3$) applied in deaerated ACN. The spectra were recorded in situ with a spectroelectrochemical cuvette (1 mm optical path). $c = 3.0 \times 10^{-4}$ M, 25 °C.

## 8. Femtosecond Transient Absorption (fs-TA) Spectroscopy

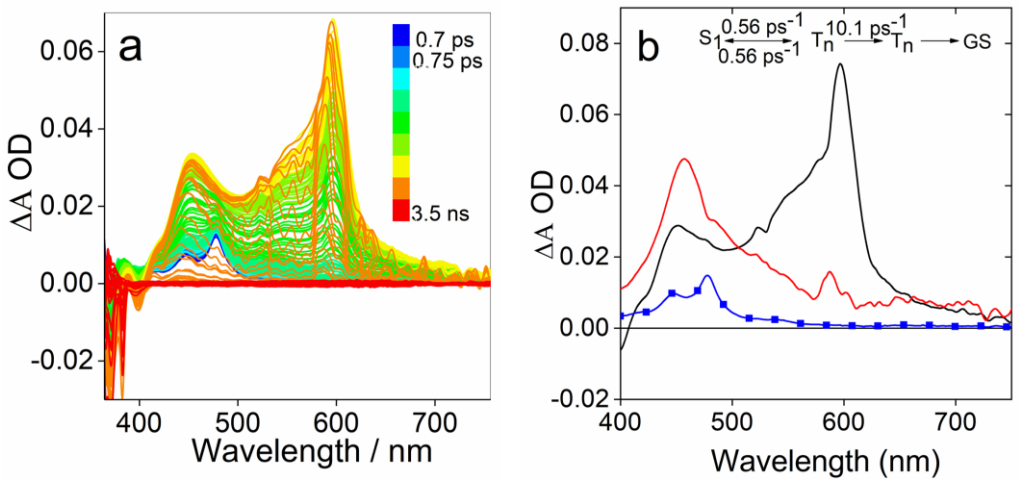


**Figure S17.** (a) Femtosecond transient absorption spectra of **NDI** in ACN, (b) SADS (Species associated difference spectra) obtained with target analysis using the kinetic scheme depicted on top.

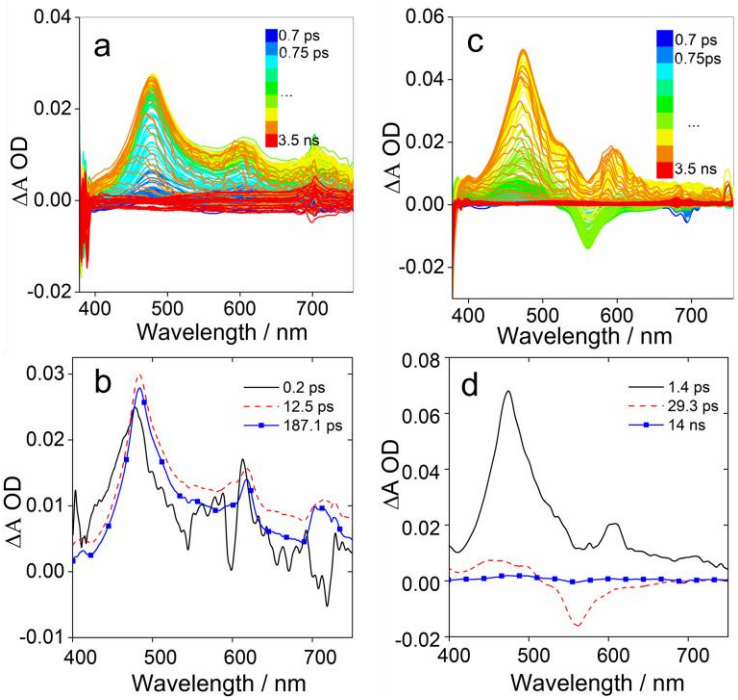


**Figure S18.** Femtosecond transient absorption spectra of **Rho-NDI** in (a) HEX, (c) ACN. The related evolution associated difference spectra obtained from global analysis with a sequential model in (b) HEX and (d) ACN.

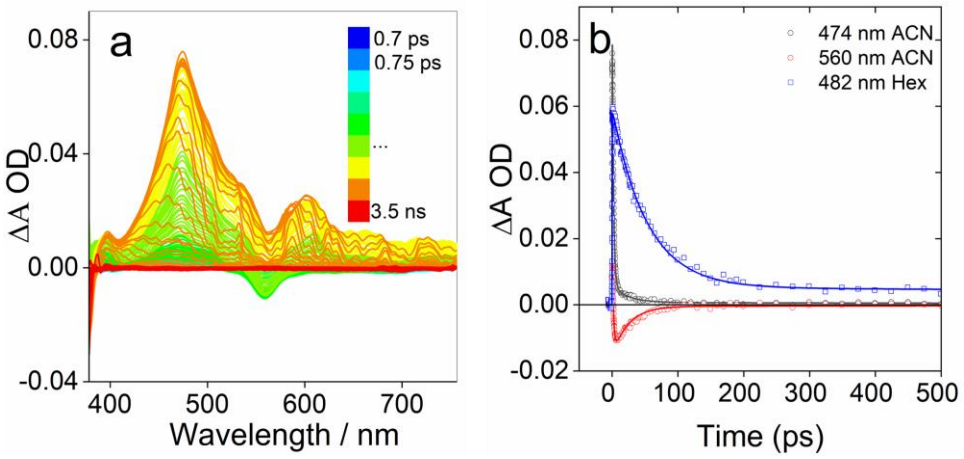


**Figure S19**. (a) Femtosecond transient absorption spectra of **Rho-NDI-Rho** in ACN. (b) kinetic traces recorded on the maximum of two solvents.

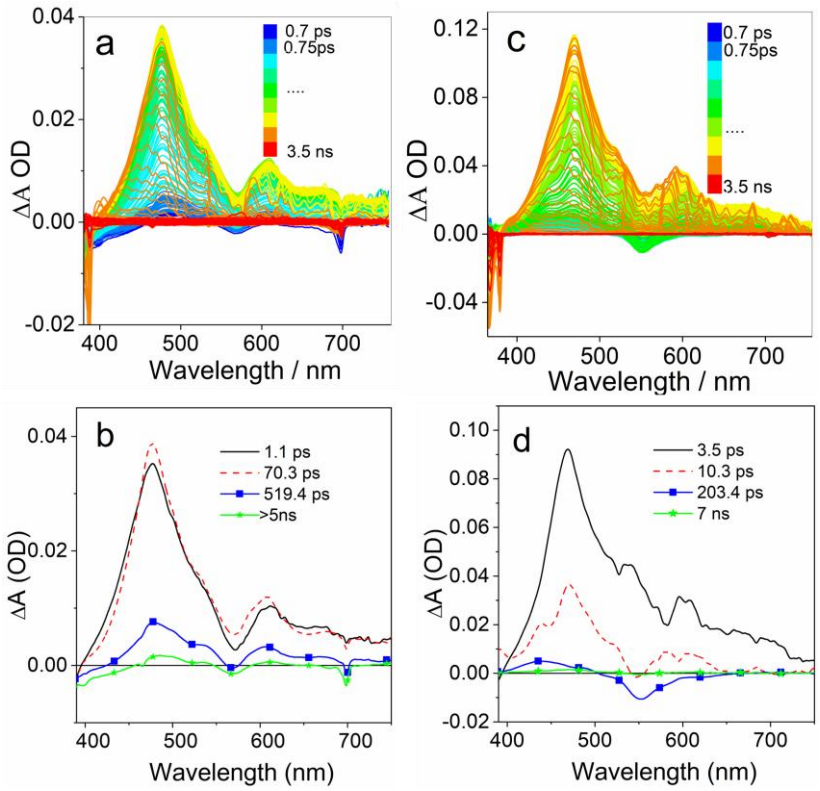


**Figure S20.** Femtosecond transient absorption spectra of **Rho-CH-NDI-CH-Rho** in (a) HEX, (c) ACN. The related evolution associated difference spectra obtained from global analysis with a sequential model in (b) HEX and (d) ACN.

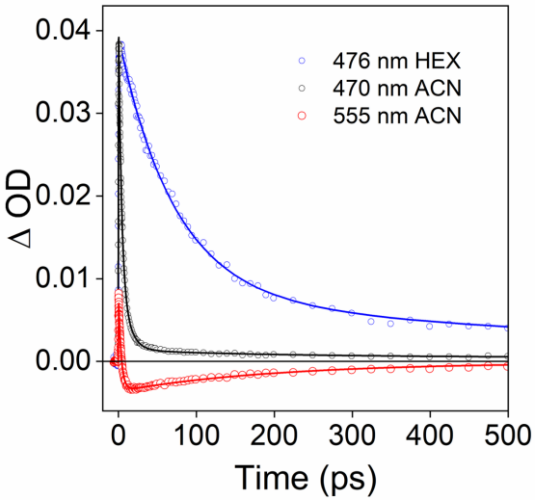


**Figure 21**. Femtosecond transient absorption spectra of **Rho-CH-NDI-CH-Rho** in kinetic traces recorded on the maximum of two solvents.

**9. Nanosecond Time-Resolved Transient Absorption Spectroscopy**

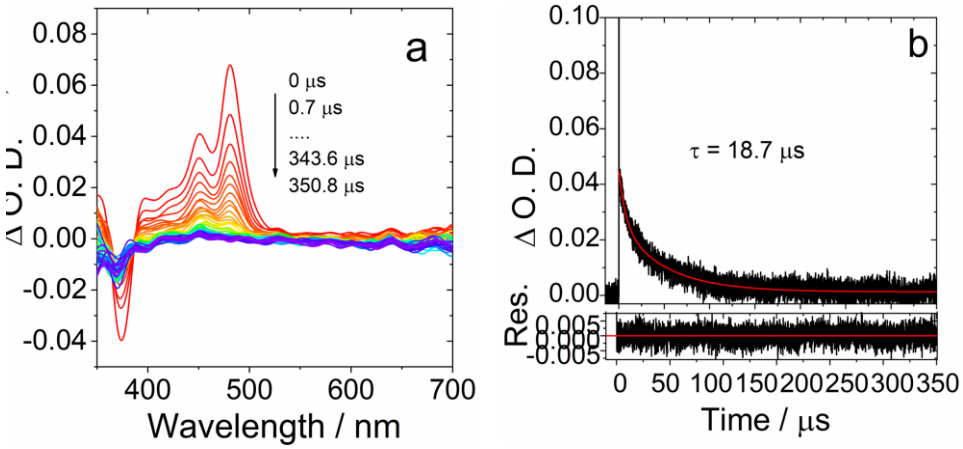


**Figure S22.** Nanosecond transient absorption spectra of **NDI** in deaerated (a) HEX. (b)The decay traces of **NDI** deaerated HEX. at 470 nm, $\lambda_{ex}$ = 355 nm, $c$ = 3.0 × $10^{-5}$ M, 25 °C.

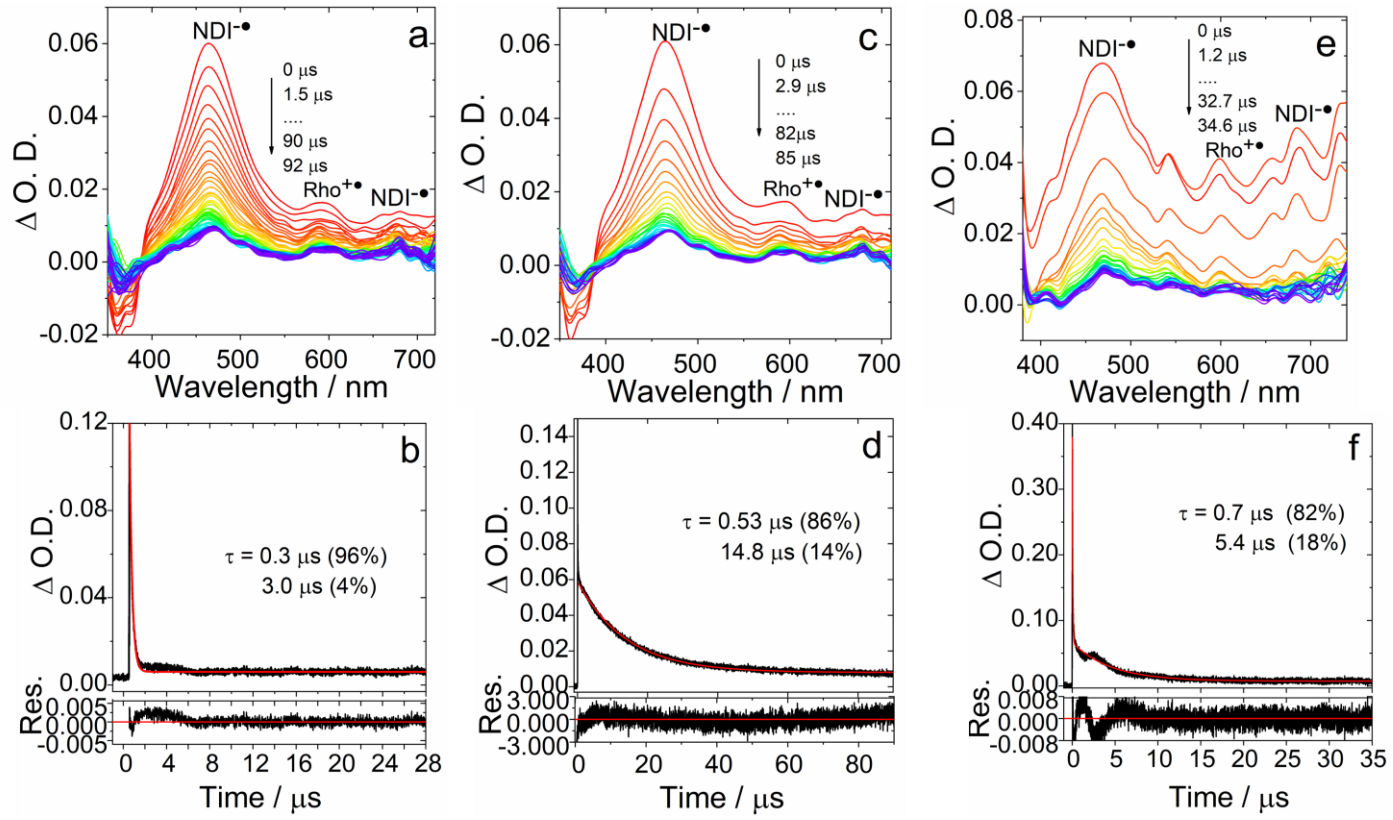


**Figure S23.** Nanosecond transient absorption spectra of (a) **Rho-NDI-Rho**, (c) **Rho-CH-NDI** and (e) **Rho-CH-NDI-CH-Rho** in deareated viscous solvent dimethylsilicone oil 500. The decay traces of (b) **Rho-NDI-Rho**, (d) **Rho-CH-NDI** and (f) **Rho-CH-NDI-CH-Rho** deaerated dimethylsilicone oil 500 at 480 nm, $\lambda_{ex}$ = 355 nm, $c$ = 5.0 × $10^{-5}$ M, 25 °C.

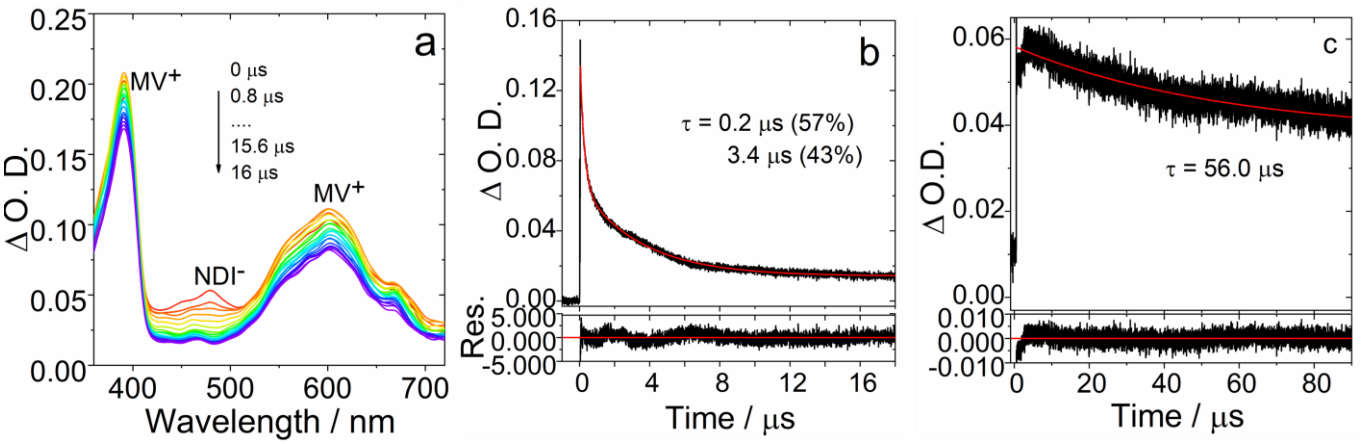


**Figure S24.** (a) Nanosecond transient absorption spectra of quenching of the radical anion of **Rho-CH-NDI** in ACN ($MV^{2+}$ as electron acceptor), (b) decay trace of radical anion at 470 nm, (c) decay trace of radical $MV^{\bullet+}$ at 600 nm.

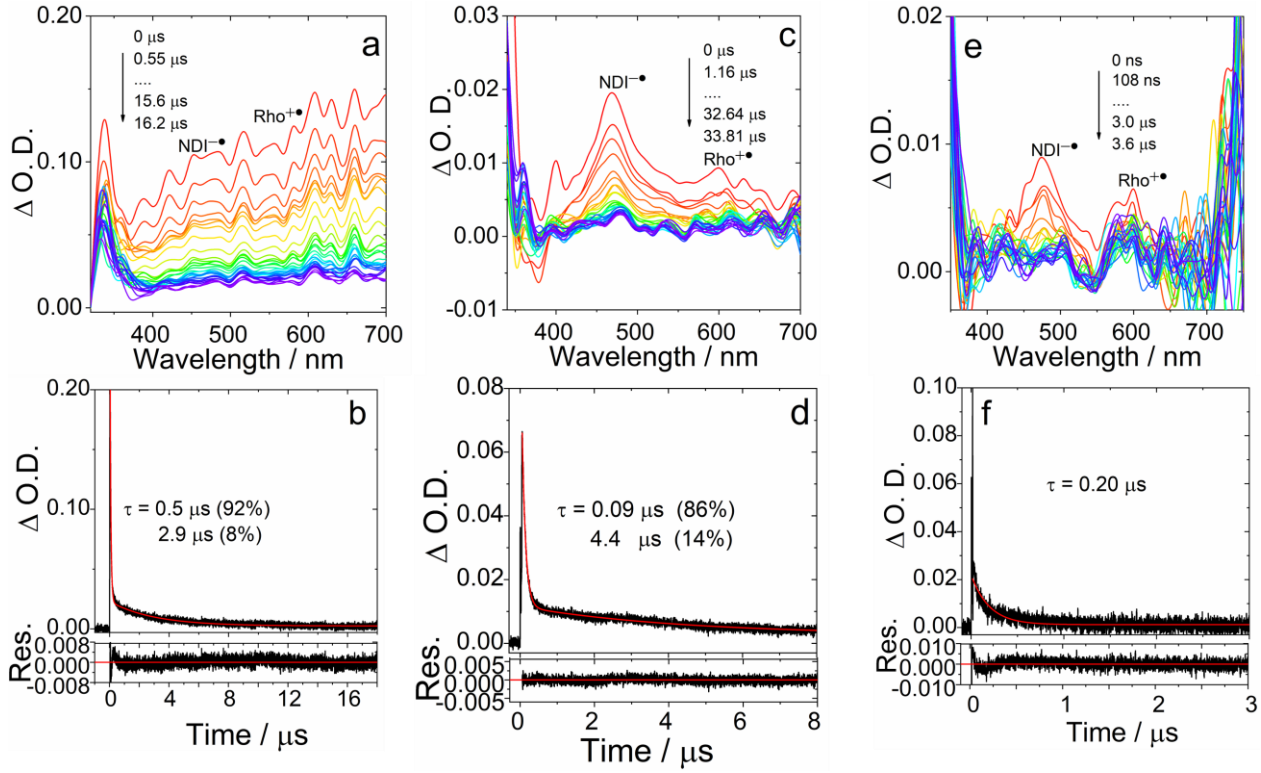


**Figure S25.** Nanosecond transient absorption spectra of **Rho-CH-NDI-CH-Rho** in deaerated (a) HEX, (c) TOL, (e) ACN. The decay traces of **Rho- CH-NDI-CH-Rho** deaerated (b) HEX, (d) TOL, (f) ACN at 470 nm, $\lambda_{ex}$ = 355 nm, $c$ = 3.0 × $10^{-5}$ M, 25 °C.

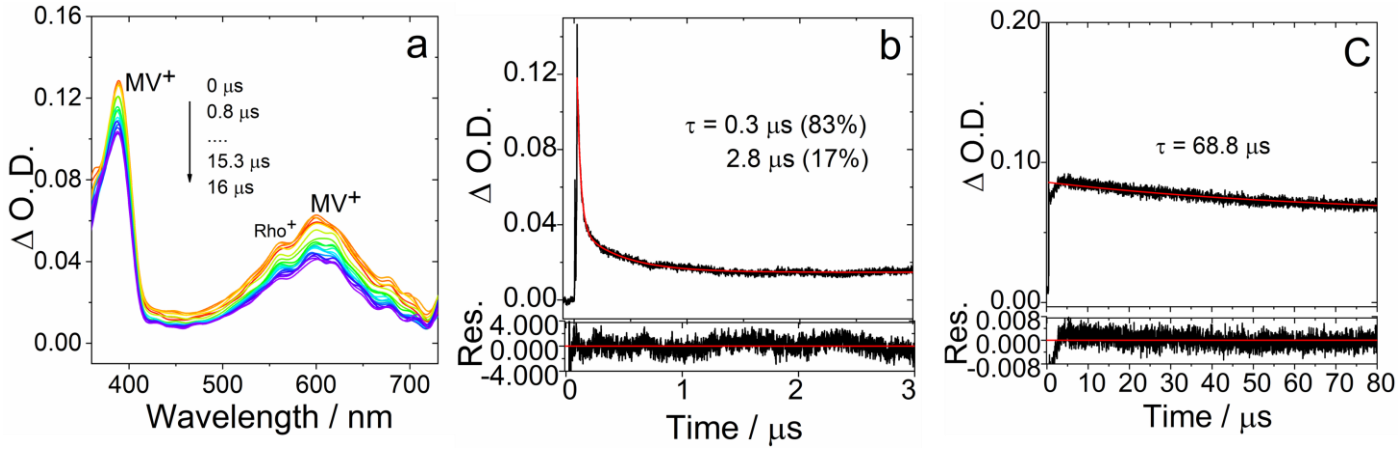


**Figure S26.** (a) Nanosecond transient absorption spectra of quenching of the radical anion of **Rho-CH-NDI-CH-Rho** in ACN ($MV^{2+}$ as electron acceptor), (b) decay trace of radical anion at 470 nm, (c) decay trace of radical anion at 600 nm.

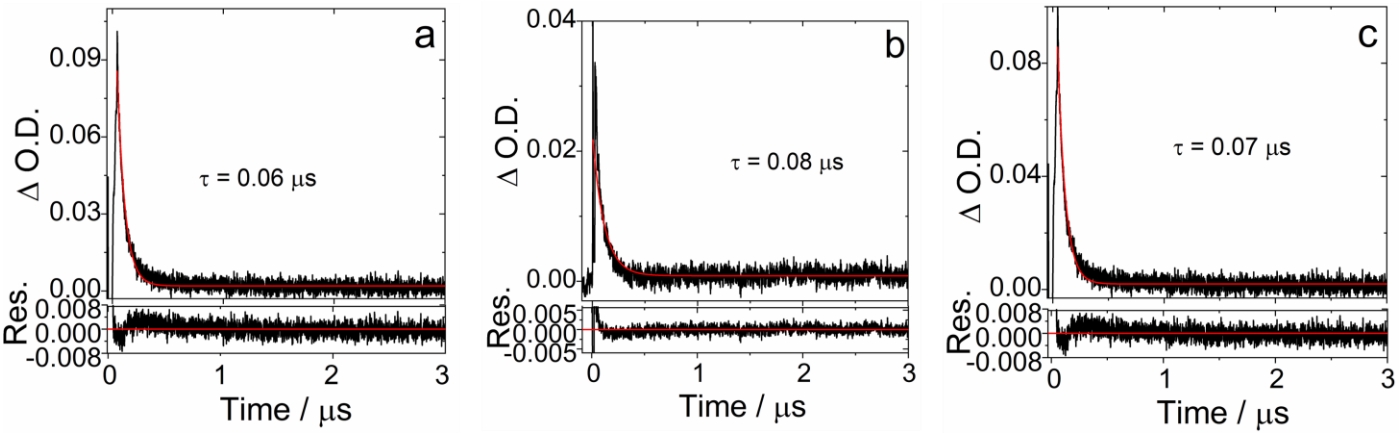


**Figure S27.** The decay traces of **Rho-NDI-Rho** in aerated (a) HEX, (b) TOL and (c) ACN at 480 nm, $\lambda_{ex}$ = 355 nm, $c$ = 3.0 × $10^{-5}$ M, 25 °C.

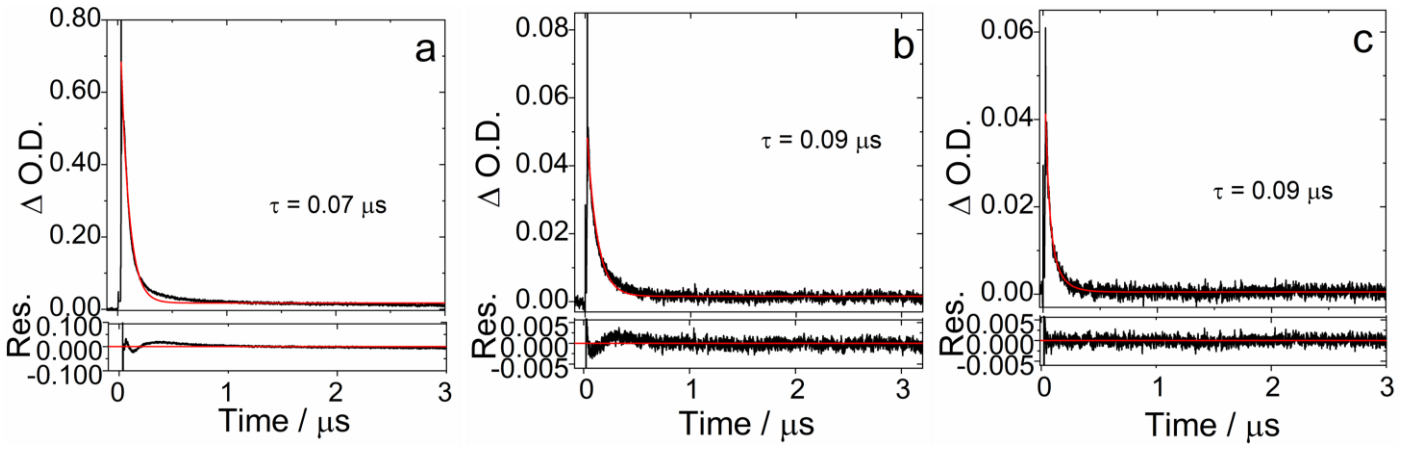


**Figure S28.** The decay traces of **Rho-CH-NDI-CH-Rho** in aerated (a) HEX, (b) TOL and (c) ACN at 470 nm, $\lambda_{ex}$ = 355 nm, $c$ = 3.0 × $10^{-5}$ M, 25 °C.

## 10. Time-Resolved Electron Paramagnetic Resonance (TREPR) Spectroscopy.

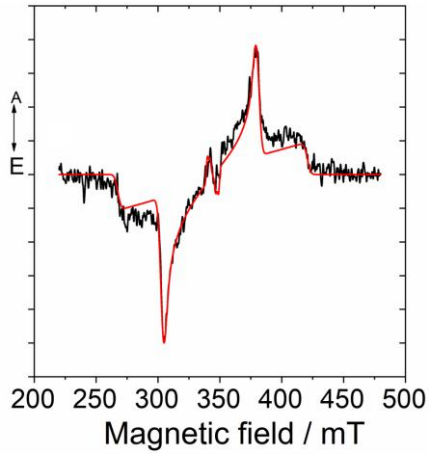


**Figure S29.** TREPR spectra of **Rho-CH-NDI-CH-Rho** in TOL/2-MeTHF (3:1, v/v). $c$ = 3.0 × $10^{-5}$ M. The black lines represent the experimental data, while the red lines correspond to the simulated spectra.

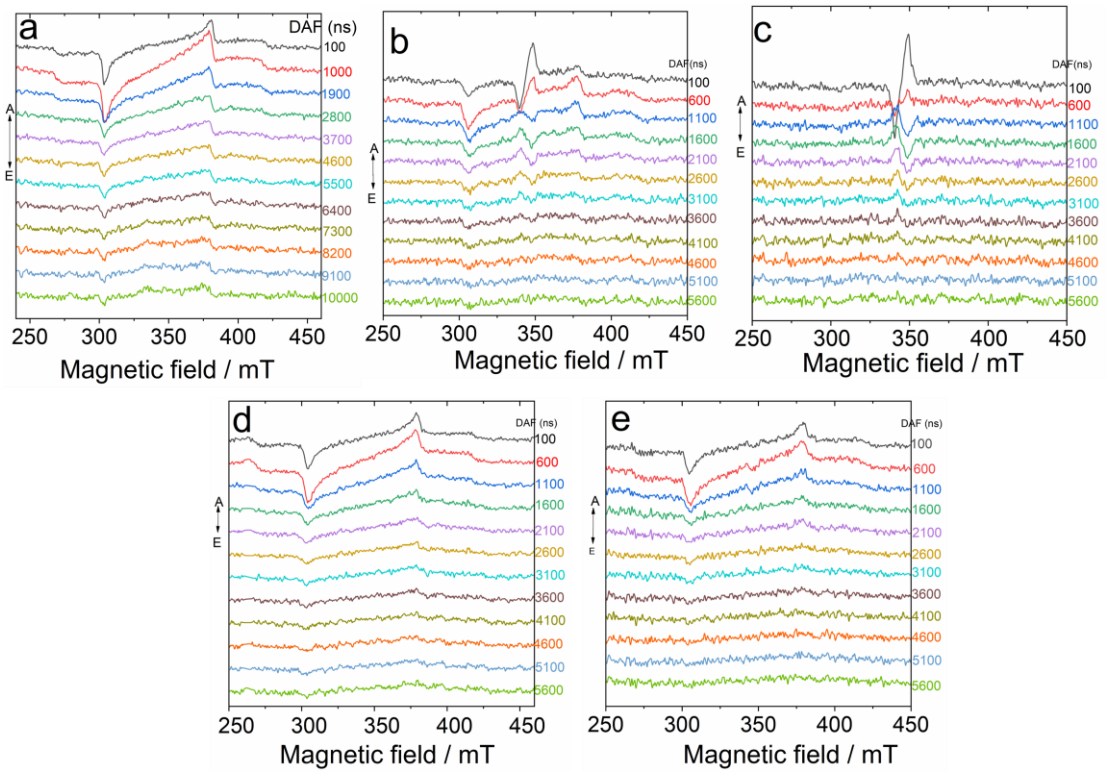


**Figure S30.** TREPR spectra of (a) **NDI**, (b) **Rho-NDI**, (c) **Rho-NDI-Rho**, (d) **Rho-CH-NDI** and (e) Rho-**CH-NDI-CH-Rho**. The spectra were obtained under laser irradiation at 80 K in glassy touene/2-me-tetrahydrofuran = 3:1 (v:v) $c$ = 3.0 × $10^{-5}$ M.

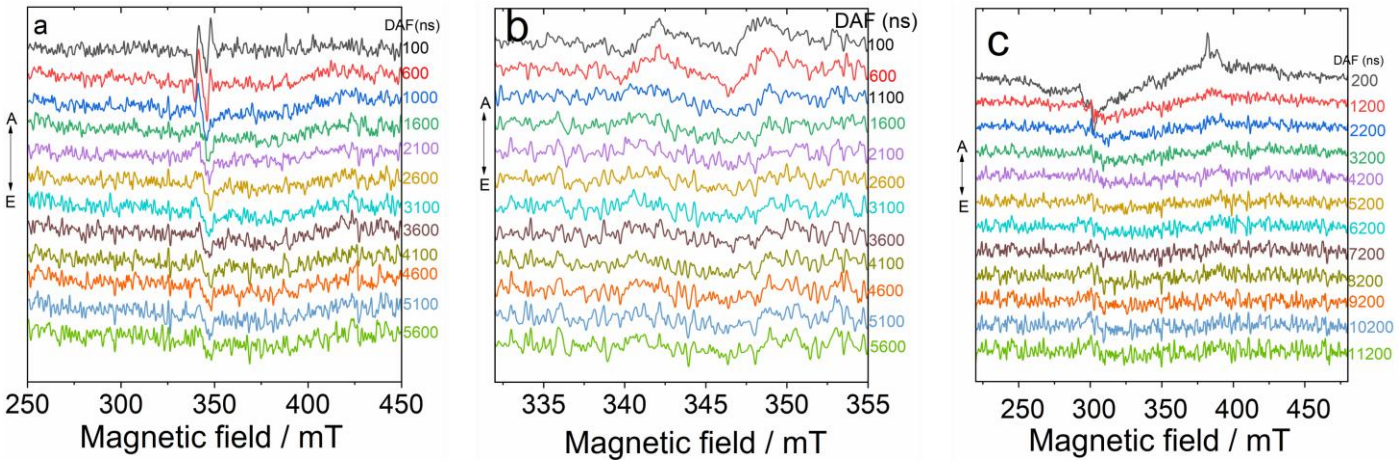


**Figure S31.** TREPR spectra of (a) **Rho-NDI**, (b) **Rho-NDI-Rho** and (c) **Rho-CH-NDI**. The spectra were obtained under laser irradiation at 80 K in glassy DCM/2-me-tetrahydrofuran = 1:1 (v:v) $c$ = 3.0 × $10^{-5}$ M.

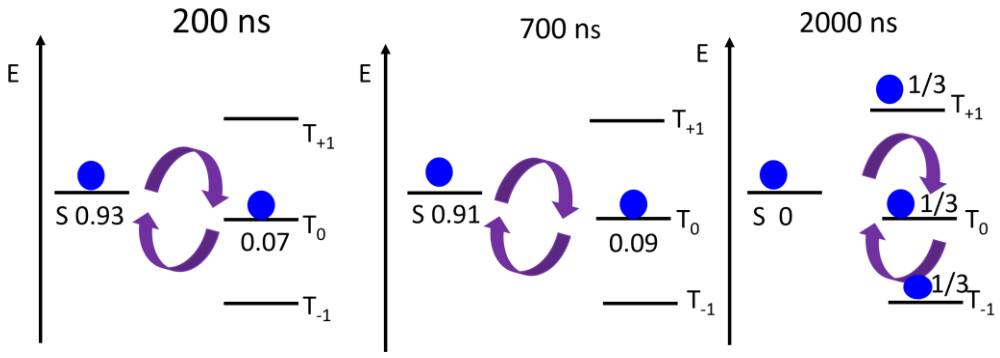


**Figure S32.** Triplet state formation in a radical pair system initially in the singlet excited state occurs via singlet–triplet (S/$T_0$) mixing. This S/$T_0$ mixing is energetically favorable, facilitating population transfer between the singlet and triplet states, as indicated by the arrows.

## 11. DFT Calculations

**Table S4**. Hyperfine Coupling Constant of $NDI^{-\bullet}$ of the Triads and Reference Compounds by Simulating the EPR Spectra and DFT Calculation (B3LYP/EPR-II)

| HFC constant/G | | $\alpha_{N1}$ | $\alpha_{N1}$ | $\alpha_{H1}$ | $\alpha_{H2}$ | $\alpha_{H3}$ | $\alpha_{H4}$ |
|---|---|---|---|---|---|---|---|
| **NDI** | Sim. | 0.99 | 0.99 | 1.86 | 1.86 | 1.86 | 1.86 |
| | DFT | 1.03 | 1.04 | 1.82 | 1.82 | 1.87 | 1.87 |
| **Rho-NDI** | Sim. | 1.03 | 0.98 | 1.98 | 1.98 | 1.82 | 1.82 |
| | DFT | 1.07 | 1.01 | 1.95 | 1.95 | 1.76 | 1.76 |
| **Rho-CH-NDI** | Sim | 0.91 | 0.90 | 1.80 | 1.80 | 1.69 | 1.69 |
| | DFT | 0.91 | 0.90 | 1.74 | 1.74 | 1.65 | 1.65 |

## 12. Photophysical Process

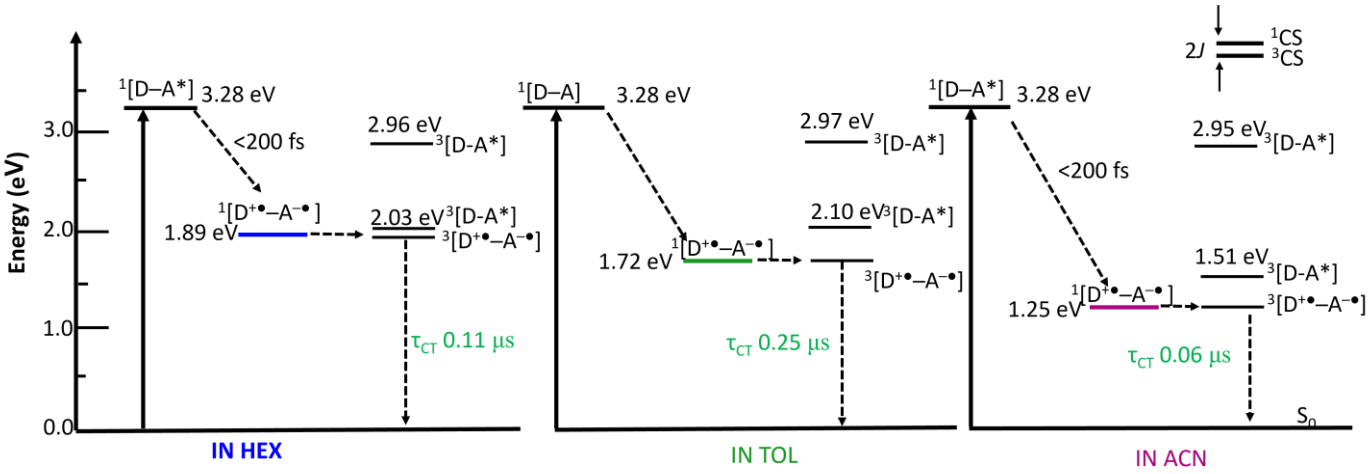


**Scheme S1** Simplified Jablonski diagram representing the photophysical process involved in **Rho-NDI-Rho** in different solvents. The $^1$[D–A*] energy levels were estimated using the singlet excited state localized on the NDI unit, determined by the intersection of the normalized UV-vis absorption and fluorescence emission spectra. The $^1$CS energy level are obtained from the electrochemical date in Table 3. The energy levels of the triplet states were taken from TDDFT calculations at the B3LYP/6-31G(d) level with Gaussian 16. *J* represents the electronic exchange energy, and the energy gap between the $^1$CS and $^3$CS states corresponds to 2*J*. The numbers in superscript designate the spin multiplicity.

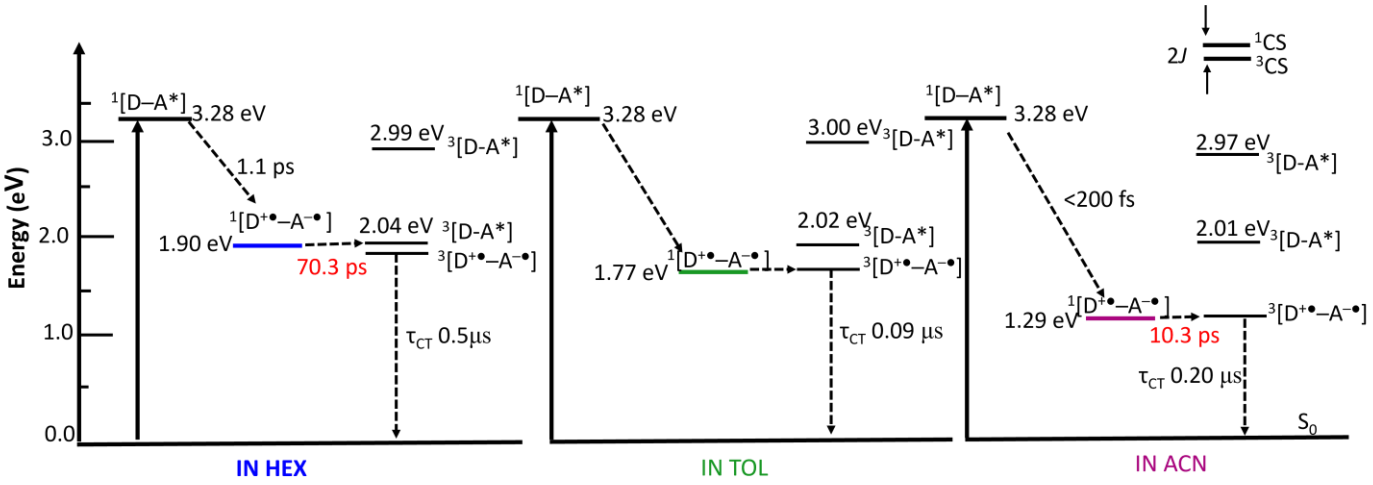


**Scheme S2**. Simplified Jablonski diagram representing the photophysical process involved in **Rho-CH-NDI-CH-Rho** in different solvents. The $^1$[D–A*] energy levels were estimated using the singlet excited state localized on the NDI unit, determined by the intersection of the normalized UV-vis absorption and fluorescence emission spectra. The $^1$CS energy level are obtained from the electrochemical date in Table 3. The energy levels of the triplet states were taken from TDDFT calculations at the B3LYP/6-31G(d) level with Gaussian 16. *J* represents the electronic exchange energy, and the energy gap between the $^1$CS and $^3$CS states corresponds to 2*J*. The numbers in superscript designate the spin multiplicity.

## 13. References


1 Y.-S. Zhang, R. Balamurugan, J.-C. Lin, S. Fitriyani, J.-H. Liu and A. Emelyanenko, *Analyst*, 2017, **142**, 1536−1544.

2 X. Xiao, I. Kurganskii, P. Maity, J. Zhao, X. Jiang, O. F. Mohammed and M. Fedin, *Chem. Sci*, 2022, **13**, 13426−13441.

3 O. V. Dolomanov, L. J. Bourhis, R. J. Gildea, J. A. Howard and H. Puschmann, *Applied Crystallography*, 2009, **42**, 339−341.

4 M. J. Frisch, G. W. Trucks, H. Schlegel, G. E. Scuseria, M. A. Robb, J. R. Cheeseman, G. Scalmani, V. Barone, G. A. Petersson and H. Nakatsuji, et al., *Gaussian 16*, Rev. C. 01, Gaussian, Inc., Wallingford, CT. 2016.

5 J. J. Snellenburg, S. Laptenok, R. Seger, K. M. Mullen and I. H. Van Stokkum, *J. Stat. Softw.*, 2012, **49**, 1−22.

6 S. Stoll and A. Schweiger, *J. Magn. Reson.*, 2006, **178**, 42—55.